The Integrated Multiscale Modeling of Diamond Chemical Vapor Deposition

David J. Srolovitz, David S. Dandy, James E. Butler, Corbett C. Battaile, and Paritosh

The fundamental mechanisms of diamond growth occur on the atomic scale; however, the geometry of the deposition reactor and the other operating parameters directly affect the chemical composition of the gas and the temperature at the growth surface. The properties are, in turn, controlled by both atomic- and microstructural-scale features. By developing diamond-growth models at each length scale and coupling the output of one model into the next, a comprehensive simulation scheme for diamond deposition is realized. This approach provides the missing link between chemical vapor deposition reactor design/operating conditions and the material structure/properties.

INTRODUCTION

The cost-effective implementation of advanced materials processing lies at the core of numerous emerging technologies. Many of these materials and structures require chemical- and plasma-driven deposition and etching processes for fabrication. It is both desirable and often necessary to develop a detailed understanding of the mechanisms of vapor processing, including the impact of defects, impurities, and morphology on the critical properties desired for the application and the overall cost of the process. The chemical vapor deposition (CVD) of diamond and diamond-like materials[1-5] is an example of a vapor-processing technique that has all of the complexity and issues of these processes. On the other hand, it benefits from the theoretical simplicity of carbon and from the knowledge base of organic and combustion chemistry.

The properties of diamond are quite extreme compared with other materials. These include the highest hardness, thermal conductivity, and chemical-corrosion resistance as well as a very large optical transmission range, electrical band gap, and insulation strength. In addition, diamond exhibits small friction and thermal-expansion coefficients and dielectric constants.[6] It is the unique combinations of these properties that make diamond a desirable material for complex cutting tools, thermal management and active devices for high-power and high-frequency electronics, corrosion- and radiation-durable components, low-friction and wear-resistant parts, and durable electrochemical electrodes and sensors, among many other applications.

In the last decade, the CVD of diamond materials has become commercially viable. These CVD diamonds range from nanocrystalline films, through large-area thick polycrystalline plates, to thin homoepitaxial single-crystal films with a continuum of qualities varying from nearly defect-free (white or optically clear) material to highly defective but mechanically tough (black) material. The CVD process has enabled the engineering of complex shapes (e.g., domes, fibers, tubes) and large sizes (up to 30 cm in diameter), something never before possible using natural diamonds or synthetic diamond grown in high-pressure, high-temperature presses. The commercialization of these materials is still limited by many factors. The dominant limitations include the deposition cost, which is controlled by the relatively low mass-deposition rate and the sizable capital equipment costs, and the lack of a detailed understanding of the deposition process that is required to achieve optimal process control.

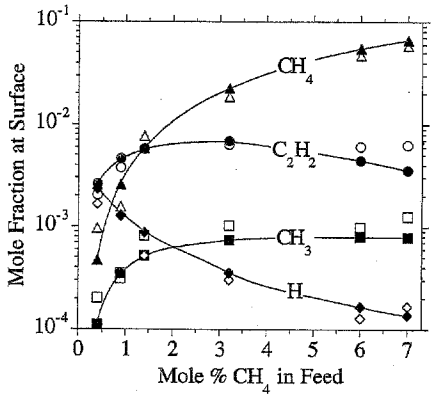

Figure 1. Modeled[14] (solid symbols) and experimental[45] (open symbols) gas-phase species concentrations at the growth surface as a function of the concentration of methane in the feed gas.

The scientific and technical understanding of diamond CVD processes has progressed significantly to the point where the generic mechanisms by which diamond is deposited at pressures and temperatures at which it is thermodynamically metastable are well understood.[7-10] Many of the complex gaseous reactions and species-transport issues have been studied and addressed.[11-13] However, the detailed knowledge of the specific stereochemical surface reactions that control film morphology, crystallographic texture, roughness, microstructure, and defect/impurity incorporation is still lacking. All of these issues are critical for controlling film properties and processing.

In-situ observations and measurements of this complex growth process are extremely difficult, particularly at the level of determining specific reaction mechanisms and pathways or spatially resolving temperatures and compositions.[16] Still, in-situ measurements have been critical in providing insight into the complexity and nature of the deposition process.[17] These measurements have been extremely valuable in determining which gaseous species are present near the growing surface, understanding the transport of gaseous species in the reactors, determining macroscopic growth rates, giving measures of material quality, and providing the factual framework that constrains the models used to express our un-

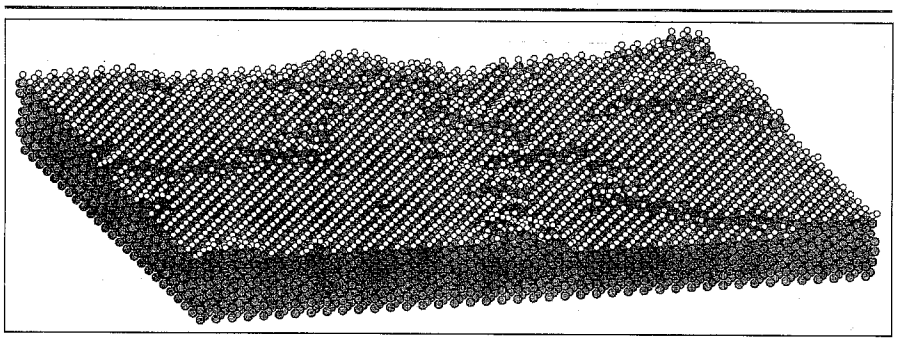

Figure 2. The atomic structure of a stepped (111) diamond surface of 100 nm² cross-sectional area for conditions typical of hot filament reactors (0.4% methane feed at 1,100 K). Gray and white atoms are carbon and hydrogen, respectively.

derstanding of the deposition process.

Valuable information about the growth process has been obtained from ex-situ examination of deposited films by correlating the morphology of the crystalline material and the defects incorporated in the material with the growth conditions. Surface chemical studies of single-crystal surfaces in ultrahigh vacuum have also played a significant role in understanding the surface structure and chemical species.[18–20]

Mathematical/computational models of the deposition process provide valuable new tools to the materials community. Detailed models of the CVD process must cover lengths from the dimensions of atoms and molecules (0.1 nm) to the size of the reactor (0.1–1 m) and temporal dynamics of the process from 10–13 seconds (atomic motion) to the hours and days required to build up bulk material (10^2–10^5 s). Thus, the development of an integrated model of the process must span a challenging ten orders of magnitude in length and more than 15 orders of magnitude in time. The tremendous advances in computational hardware have enabled the development and use of sophisticated computational models to gain insight into many elements of this process at levels either difficult or impossible to access experimentally, such as the details of gas species transport, temperature distributions, plasma chemistry, atomic-scale stress distributions, grain growth, and defect incorporation. It has also enabled the ab initio computation of specific reaction rates (cross sections), energetics, and mechanisms based on the fundamental interactions occuring between atoms and molecules.

The goal of this work is to develop an integrated set of tools (models) that enables a detailed understanding of the vapor processing of materials. The models are divided into three loose categories that address the chemical kinetic reaction and transport of gaseous species to/from the growing film (macroscale), the geometrical modeling of the microstructural and morphological evolution (microscale), and molecular and atomic simulations of the growing film (nanoscale). Reactor-scale models focus on the rector hydrodynamics and the gas-phase and gas-surface chemistry and predict the temperature and composition profiles. This information is used as input to a molecular-scale simulation of diamond film growth that self-consistently predicts the rates of growth of individual surface orientations. The growth rates predicted by the molecular-scale model are then input to a front-tracking model of microstructural evolution in polycrystalline films that yields information about film morphology, crystallographic texture, and grain size.

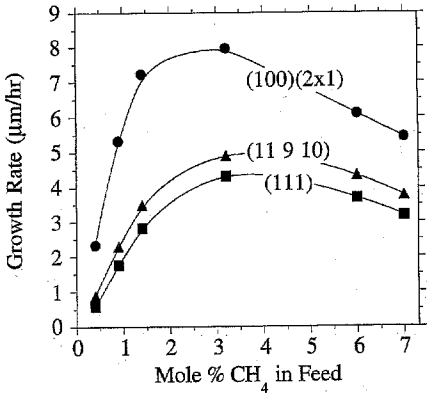

Figure 3. Growth rates of (100)(2 x 1), (111), and near-(111) oriented films as a function of the concentration of methane in the feed gas.

The close coupling of the model predictions with experimental observations and constraints is critical to the development of robust models of the growth process and the optimization and control of material quality/costs. Ideally, all of the inputs to the models at all levels would be derived from experiments or experimentally verified calculations. Realistically, this is nearly impossible to do with available resources, so input data obtained from less fundamental models is often used, which are validated using prudently selected experiments. A background on the modeling methods employed is described in the sidebar.

REACTOR-SCALE MODELING

A significant factor complicating reactor models is the presence of the energy source. Whether it is the arc jet issuing from a d.c. plasma torch, the hot-filament(s), or the microwave or RF plasmas, assumptions must invariably be made in constructing a physical model of the source. Not surprisingly, the particular assumptions strongly affect the predicted temperature and species distributions within the reactor.

Most hot-filament reactor modeling efforts have concentrated on determining the temperature profile and, in particular, the species distribution in the region between the filament and substrate to identify likely diamond-growth precursors and develop and validate deposition mechanisms. The models have also been used to examine the role played by the filament in initiating gas-phase chemistry. Theoretical studies of hot-filament reactors may be roughly divided according to whether one- or two-dimensional models were used. The

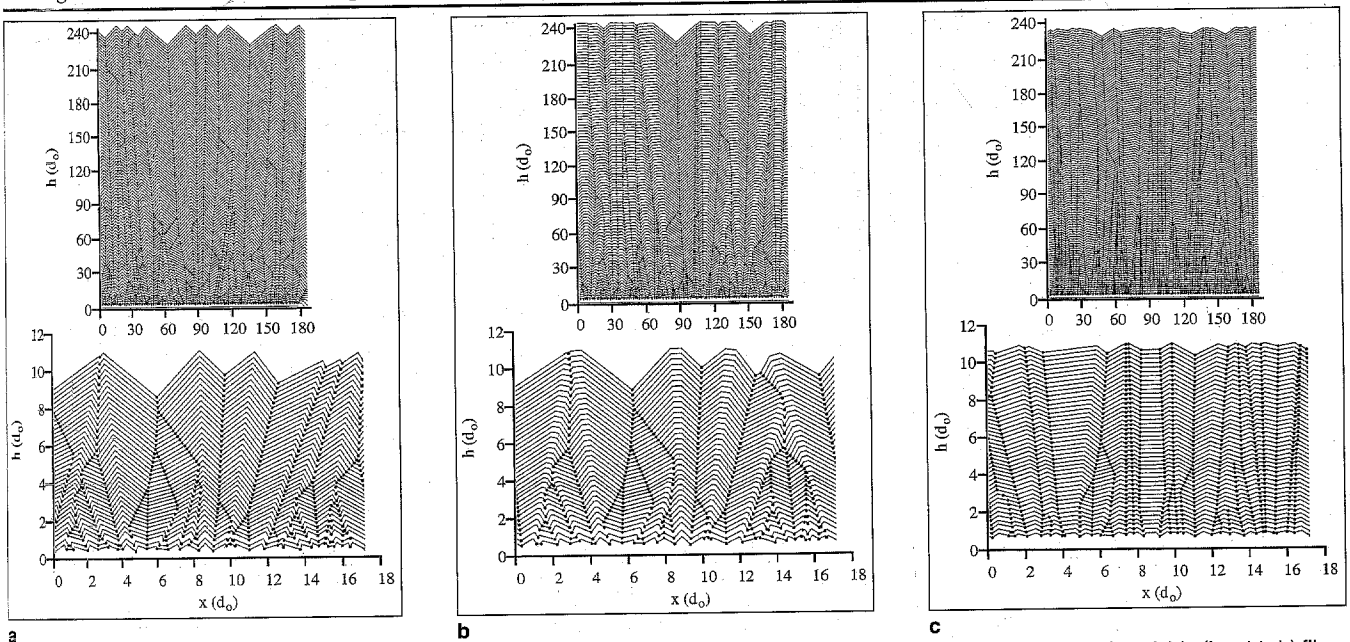

Figure 4. The microstructures of polycrystalline diamond films at (a) $\alpha = 2.0$, (b) $\alpha = 1.95$, and (c) $\alpha = 1.5$. Thick ($h = 226\ d_o$) and thin ($h = 11\ d_o$) films are shown for each α (where d_o is the average initial nucleus separation). The solid and dotted lines indicate the evolution of the growth front and the grain boundaries, respectively.

one-dimensional models typically include detailed gas-phase and gas-surface chemistry and have been used to gain insight into the chemical kinetics governing diamond deposition and the relationship between mass transfer and chemistry.[14,24] An example of a comparison between theory and experiment is shown in Figure 1, where the gas-phase composition at the substrate is plotted against the fraction of CH_4 in the feed-gas mixture. The modeled reactor conditions correspond to a 2,620 K hot filament positioned 1.3 cm from the 1,073 K growth surface in a chamber at 20.25 Torr with a mixture of CH_4 and 7 vol.% argon in H_2 fed into the growth chamber at 1 cm/s axial velocity.[14] The molecular-beam mass spectrometry data were taken by sampling through a pin hole in the substrate center.[45] Quantitative agreement such as that between the modeled and measured species concentrations in Figure 1 has lent confidence to the ability of detailed chemical kinetic and transport models to accurately simulate diamond deposition. Limited studies have been performed on developing two-dimensional models; these generally contain simplified gas-phase chemistry[30] and often do not contain deposition mechanisms. These models yield information on the details of mass, momentum, and energy transport in reactors.[28,46]

A lack of quantitative data for temperature and composition in d.c. arc-jet, RF plasma, and microwave plasma reactors have led investigators to use models to predict macroscopic observables such as film growth rate and examine near-substrate gas composition for potential growth precursors. As in the studies of hot-filament systems, most models of d.c. and RF arc-jet reactors have been one-dimensional, based on uniform stagnation or uniaxial straining flow assumptions, and have included detailed homogeneous and heterogeneous chemistry.[13,47] Although the one-dimensional models predict gas-phase temperature and composition as functions of distance above the substrate and deposition rates, at present, no published experimental data for these quantities exist. In lieu of such comparisons, the models have been applied to investigate potential diamond-growth precursors by contrasting predicted fluxes of specific hydrocarbon species with experimental film-growth-rate data.

Inroads have been made in applying two-dimensional models to d.c. arc-jet systems. Mankelevich et al.[29,48] included

MODELING METHODS: A BACKGROUND

Modeling Reactor-Scale Processes

Numerical and analytical solutions of the continuum equations governing the conservation of momentum (fluid flow), mass, and energy (temperature) have led to many insights into the mechanisms and conditions under which diamond may be grown by CVD. Modeling many types of diamond reactors has proven successful primarily because the principle hydrocarbon sources used are CH_4 and C_2H_2, and the pyrolysis and combustion mechanisms for these fuels are well understood for the stoichiometries used.[21-23] Thermodynamic and thermophysical data for the various gaseous species are known.

The reactor configurations and operating conditions used in direct current (d.c.) arc-jet, radio frequency (RF) plasma, combustion, and hot-filament systems often lend themselves to geometric simplifications that, in turn, make the numerical models tractable, even with detailed homogeneous and heterogeneous chemistry. One-dimensional models of these reactors have proven successful in describing qualitative (e.g., composition and temperature profiles) and quantitative (e.g., diamond growth rate) features in systems where charged species (plasma) chemistry does not play a significant role.[13,14,24-27]

More detailed modeling that captures multidimensional effects and ion-neutral chemistry is still required in order to adequately describe systems containing nonthermal plasmas (e.g., microwave reactors). Most recently, two-dimensional calculations have focused on momentum and heat transport in reactors[11,28] and omitted detailed chemical kinetics models. However, two-dimensional models with reduced homogeneous and heterogeneous chemical mechanisms were recently developed for d.c. arc-jet[29] and hot-filament reactors.[30]

Because of the difficulties that are involved in modeling nonthermal plasma systems, fewer theoretical studies have been performed on microwave reactors.[31] One exception is a simplified two-dimensional microwave reactor[32] that couples zero-dimensional calculations of the electron-energy distribution to transient equations describing ion and neutral species chemistry.

A driving force for the development of more complex reactor models is the knowledge that the properties of diamond films and their microstructure are integrally related. By definition, the continuum-reactor models cannot address crucial issues such as morphological evolution, defect formation, and grain growth. The continuum models provide one-dimensional predictions of the growth rate, but are incapable of directly incorporating microscopic information into the model or predicting any quantities that are microstructure dependent.

Simulating Growth on the Atomic Scale

Most previous attempts to model the growth of diamond films are based on chemical kinetic analyses of the rates of production of various species on the growth surface.[9,13,31-35] While this approach is useful for testing proposed growth mechanisms and estimating growth rates, it accounts only for the chemistry of diamond growth and not for the evolving atomic structure of the diamond surface. These methods cannot be used to predict film morphologies and defect densities, and the transfer of chemical kinetic growth models from one type of surface to another is not straightforward. The prediction of atomic and structural information and the self-consistent calculation of the properties of different film orientations can be accomplished by combining the surface-reaction chemistry used in conventional growth models with a realistic three-dimensional atomic representation of the film. This approach has been adopted in two recent studies,[36,37] but only to predict growth rates and morphologies of individual surface orientations. One of the benefits these models—the self-consistent comparative study of diamond growth on different surface orientations—is only now being explored.

In contrast to a reactor-scale model, atomic-scale models are able to predict the growth velocities for surfaces of any orientation, vacancies incorporation, and surface reconstruction. Such models require detailed knowledge of the flow field, temperature, and composition in the gas adjacent to the deposition surface. Thus, there is a tight coupling between the reactor-scale models and the atomistic models. For a given set of operating conditions, the reactor-scale models may be used to produce a two-dimensional map of gas-phase conditions at the deposition surface. The atomic-scale models, in turn, use these conditions to accurately predict microscopic growth information, such as the growth rate that may be passed back to the continuum models or forward to the microstructural models.

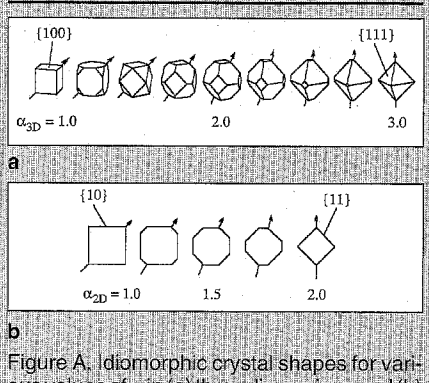

Figure A. Idiomorphic crystal shapes for various values of α in (a) three dimensions and (b) two dimensions. The arrows indicate the direction of fastest growth.

A generalized diamond-growth model of this type must treat the growth process on a level that is sufficiently fundamental to avoid restricting the model to particular surface orientations or growth conditions. This is accomplished by considering the surface chemical reactions involved in the CVD process on the molecular/atomic level and on a (surface) site-by-site basis instead of modeling configurational transitions between relatively large molecular clusters at specific surface orientations.[34-36,38] A set of basic chemical reactions that are not restricted to specific growth surfaces, but depend on local bonding configurations is adopted from kinetic models of diamond growth and coupled to the three-dimensional atomic-film model.

The set of reactions used in this study is provided in Table 1[33,34,39] and is general enough to allow growth at arbitrary surface orientations and atomic surface features. Table 1 contains the forward-rate coefficients and thermochemistry for each chemical reaction. C_d represents a surface diamond atom; species separated by a bullet (·) are dimer bonded, and an asterisk (*) represents a surface biradical. Forward-rate constants are $k_f = A\,T^n \exp(-E/RT)$ and reverse-rate constants are $k_r = C\,A\,T^n \exp(-\Delta S/R)\exp((\Delta H - E)/RT)$, where C is a constant that accounts for the fact that ΔH and ΔS correspond to a standard state of 1,200 K and 1 atm; C is equal to 1.016×10^{-3} mole · cm³/atm for reactions where the number of moles changes (i.e., the number of products and reactants are unequal) and unity otherwise. Reactions 1 and 2 involve hydrogen and the diamond surface. Reactions 3–5 occur between hydrocarbon molecules and the surface. Reactions 6–9 are between hydrogen and adsorbed hydrocarbons. Reactions 10 and 11 represent the addition of CH_2 to an adsorbed hydrocarbon. Reactions 12–15 handle hydrogen and hydrocarbon molecules interacting with dimer-bonded surface atoms. (Reactions 6–11 apply to both dimer-bonded and non-dimer-bonded.) Reaction 16 represents formation/breaking of dimer bonds between surface atoms,[36] and Reaction 17 represents insertion of a hydrocarbon into an opened dimer bond.[36]

The reaction-rate coefficients and reaction thermochemistry in Table 1 are combined with information about the densities of gas-phase species near the growth surface to determine the absolute rates of each reaction. This specifies the identities and rates of all the chemical processes that can possibly occur at all sites on a surface in a given configuration. A kinetic Monte

two irreversible, electron-assisted dissociation reactions in a gas-phase kinetic mechanism and used a closed-form expression for the flux-boundary condition of the presumed growth species, CH_3, to predict a deposition rate as a function of position on a diamond surface. However, as discussed above, less progress has been made in modeling non-thermal plasma-assisted growth. In the zero-dimensional (point) model of Hyman et al.,[32] the Boltzmann equation was coupled to transient equations describing ion and neutral species chemistry. The model was applied to predict the rate of electron-density increase and, subsequently, to predict the atomic hydrogen concentration at the center of the plasma ball. Because this was a point model, it could not include any information regarding deposition.

Analysis of combustion-flame deposition has focused on the feasibility of using different hydrocarbon fuels (e.g., CH_4, C_2H_2, and C_2H_4) and determination of the relationship between gas composition and film growth rate. As for hot-filament and plasma-assisted systems, combustion reactors have been simulated under atmospheric[25] and subatmospheric[27] operating conditions using one-dimensional stagnation flow models. To increase deposition uniformity, combustion synthesis is often carried out at relatively low pressures. An additional benefit of low-pressure deposition is an increase in the size of the flame zone, which makes it easier to implement an optical diagnostics technique such as laser-induced fluorescence in order to study the chemistry existing in this region.

ATOMIC-SCALE GROWTH SIMULATIONS

The calculation of absolute-reaction rates suitable for the kinetic Monte Carlo algorithm requires information about the environmental conditions in the growth chamber, specifically, the substrate temperature, the chamber pressure, and the concentrations of gas-phase species at the growth surface. In the present simulations, typical hot-filament reactor conditions (substrate temperature 1,073 K and chamber pressure of 20.25 Torr) were examined, and the gas-phase concentrations at the surface for these conditions were obtained directly from the reactor-scale models. The reaction-rate constants that are obtained from Table 1 in the sidebar (using the substrate temperature for T) are converted to absolute-

Carlo method can be used to simulate the temporal evolution of the growth surface according to this information.[41] An initial diamond-growth surface covered completely by hydrogen is used as the starting condition. The growth simulation is initiated by choosing one of the possible events at random (i.e., one reaction at one surface site) with a probability equal to the rate of the corresponding reaction relative to the sum of the reaction rates of all possible changes. Once an event occurs, the list of all new surface configurations is tabulated, and additional events occur according to the same prescription. This kinetic Monte Carlo simulation procedure yields a stochastic, temporal evolution of all surface species. Diamond growth by the conversion of hydrocarbon molecules to sp^3-bonded diamond material occurs whenever and wherever hydrocarbons are bonded to the film at more than one surface site. This particular Monte Carlo algorithm employs a time increment that varies from step to step and is stochastic.[41] Since the absolute rates of all Monte Carlo events (i.e., the reactions in Table 1) are known in real units (seconds), the link between Monte Carlo time (in steps) and growth time (in seconds) is straightforward. Typical simulations account for up to a billion reaction events and extend to real growth times of up to an hour.

Modeling Microstructural Evolution

Atomic-scale growth simulations can provide detailed information about the growth of single-crystal films of virtually any orientation. However, many CVD diamond films are polycrystalline. The inclusion of multiple crystallographic orientations into an atomic-scale growth simulation would be cumbersome, and the precise effects of grain boundaries on the reaction kinetics are not known. Therefore, in order to predict the evolution of the morphology, grain size, and crystallographic texture of polycrystalline diamond films, the information from the single-crystal growth simulations is used to determine the microstructural evolution of polycrystalline films.

CVD diamond exhibits mostly {100} and {111} facets.[2,42] Thus, isolated freely-growing crystals are cubo-octahedral in shape and are bounded by {100} and/or {111} faces. The crystal shape and, thus, the densities of both types of surface orientations bounding the crystal are controlled by the relative rates of growth of the two surface orientations. This information is commonly expressed by the following growth-rate parameter:[2,43]

$$\alpha_{2D} = \sqrt{3}V_{100}/V_{111}$$

where V_{hkl} is the growth rate of the {hkl} facet. This dependence of crystal shape on α_{2D} is shown in Figure A. Low values of α_{2D} (≤ 1) yield cubic crystals with {100} faces; high values (≥ 3) produce octahedral crystals with {111} faces, and intermediate values lead to cubo-octahedral crystals bounded by both surface orientations. When a continuous polycrystalline diamond film is formed by the impingement of multiple single-crystal nuclei, the microstructural properties of the film (morphology, texture, grain size, etc.) are determined by this growth-rate parameter. The rates of growth of the different facets and the orientations of the nuclei determine which grains will survive when the film thickens (i.e., the crystallographic texture) and which facet orientations will be represented on the surface (i.e., the surface morphology).

The development of microstructure during the growth of polycrystalline diamond films is modeled by geometrically accounting for the growth and impingement of randomly oriented seed crystals (i.e., nuclei).[43] Since only two surface orientations are generally observed in CVD diamonds, the microstructural model can be simplified considerably by treating the growth and impingement of two-dimensional crystals bounded by lines (instead of three-dimensional crystals bounded by planes). In the two-dimensional model, the growth rate parameter is

$$\alpha_{2D} = \sqrt{2}V_{10}/V_{11}$$

The idiomorphic crystal shape varies from a square bounded by {10} edges when $\alpha_{2D} \leq 1$, to an octagon at $\alpha_{2D} = \sqrt{2}$, to a square bounded by {11} edges when $\alpha_{2D} \geq 2$ (Figure A).

In the two-dimensional, polycrystalline, film-growth model, which is a variant of the model originally proposed by Wild et al.,[43] the starting structure consists of an array of randomly oriented seed crystals partially embedded on an inert, rigid, static substrate. Each seed crystal is initially bounded by {10} and {11} edges. The relative velocities of the {11}- and {10}-type edges (surfaces) are determined by the prescribed value of α_{2D}. At each simulation step, each pair of adjacent vertices (i.e., intersections between crystal edges, including the substrate) is examined to determine the time at which they will intersect. The simulation clock is advanced by an amount equal to the shortest intersection time of all the vertex pairs in the system. Each vertex is advanced by a vector determined by this shortest-time increment and the bounding edges' velocities. The intersecting vertex pair is reduced to a single vertex situated at the intersection point, and the crystal edge (or segment of the substrate) between the two intersecting vertices is annihilated (i.e., buried). Secondary nucleation is not allowed, and all edges of the same orientation (i.e., either {10} or {11}) grow at the same rate. This algorithm provides a simple geometrical model of polycrystalline film growth that accounts for the competitive growth of randomly oriented grains and can be used to predict the evolution of film morphology, crystallographic texture, and grain size.

Table 1. Reaction-Rate Coefficients for Diamond Growth[33,34,39]

Reaction	A (moles, cm, s)	n	E (kcal/mole)	ΔH (kcal/mole)	ΔS [cal/(mole·K)]
1. $C_sH + H \leftrightarrow C_s + H_2$	1.3×10^{4}	0	7.3	−9.9	5.3
2. $C_s + H \leftrightarrow C_sH$	1.0×10^{13}	0	0.0	−96.9	−32.8
3. $C_sCH_2 + H \leftrightarrow C_s + CH_3$	3.0×10^{13}	0	0.0	−24.6	7.9
4. $C_s + CH_3 \leftrightarrow C_sCH_3$	5.0×10^{12}	0	0.0	−70.9	−42.0
5. $C_s + C_2H_2 \leftrightarrow C_sC_2H_2$	4.5×10^{11}	0	6.9	−28.5	−1.9
6. $C_sCH + H \leftrightarrow C_sCH_{-1} + H_2$	2.8×10^{7}	2	7.7	−11.3	6.6
7. $C_sCH_2 + H \leftrightarrow C_sCH_{-1}$	1.0×10^{13}	0	0.0	−83.0	−34.1
8. $C_sC_2H + H \leftrightarrow C_sC_2H_{-1} + H_2$	9.0×10^{8}	2	5.0	−8.9	8.7
9. $C_sC_2H + H \leftrightarrow C_sC_2H_{-1}$	2.0×10^{13}	0	0.0	−47.7	−36.2
10. $C_sC_2H_2 + H \leftrightarrow C_sCH_2 + CH_3$	3.0×10^{13}	0	0.0	−24.6	7.9
11. $C_sCH + CH_3 \leftrightarrow C_sC_2H_2$	5.0×10^{12}	0	0.0	−70.9	−42.0
12. $C_s : C_2H + H \leftrightarrow C_s : C_2 + H_2$	2.5×10^{14}	0	7.3	−6.2	6.7
13. $C_s : C_2 + H \leftrightarrow C_s : C_2H$	1.0×10^{13}	0	0.0	−100.6	−34.2
14. $C_s : C_2CH_2 + H \leftrightarrow C_s : C_2 + CH_3$	3.0×10^{13}	0	0.0	−17.8	8.0
15. $C_s : C_2 + CH \leftrightarrow Cd : C_2CH_2$	5.0×10^{12}	0	0.0	−81.0	−42.2
16. $C_s : C_2 \leftrightarrow C_s + {}^{*} + C_2$	1.0×10^{13}	0	0.0	4.9	0.4
17. $C_s + {}^{*} + C_2C_2H \rightarrow C_s + C_2C_2H + Cd$	2.0×10^{13}	0	8.8	—	—

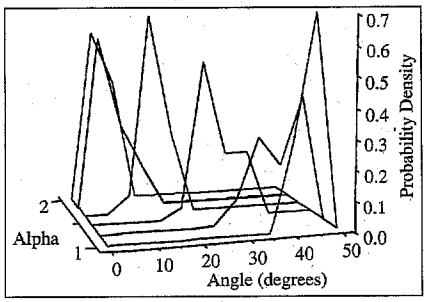

Figure 5. A series of plots of the probability distributions of grain orientations as a function of the growth-rate parameter α_{2D}. An angle of 0° corresponds to <10> texture, and 45° corresponds to <11> texture.

reaction rates using the gas-phase compositions.

One advantage of the atomic-scale model is that the formation and evolution of surface features (islands, steps, microfacets, etc.) are handled explicitly. An example of step formation during a simulation of growth on the (111) surface is shown in Figure 2. Since growth occurs atom-by-atom, the simulated surfaces develop a rich variety of surface structures and features. In addition, since growth on any surface can be simulated with the same set of chemical reactions using this method, growth behavior for different surface orientations can be predicted and compared. For example, growth rates can be calculated by monitoring the film height vs. time. Rates of growth on initially hydrogen-terminated (100) [with a (2×1) reconstruction], (111), and (11 9 10) surfaces are shown in Figure 3 for the inlet CH_4 concentrations shown in Figure 1. The (11 9 10) surface is meant to represent a substrate which is slightly miscut (by 4.7°) from (111). Growth on the (100)(2 × 1) surface is considerably faster than growth on the (111) and (11 9 10) surfaces, and the (11 9 10) growth rate is slightly higher than (111).

The rates of growth on different surface orientations depend partly on the absolute rates of the important chemical processes in Table 1. The reaction-rate coefficients in the table can be used to obtain rate constants for each reaction, and these constants can be converted into absolute rates using the partial density of the appropriate gas-phase reactant. Thus, the kinetics of diamond growth depend on the concentrations of gas-phase species (most importantly hydrogen, CH_3, and C_2H_2) at the growth surface. The data in Figure 1 provide experimentally verified predictions of these concentrations, which can serve as reliable input to the atomic-scale growth simulations to parameterize the reaction-rate constants obtained from Table 1. Figure 1 indicates that the concentrations of the growth species (CH_3 and C_2H_2) at the surface increase with increasing inlet CH_4. This leads to an increase in the growth rates. However, the hydrogen concentration decreases with increasing CH_4, and as the concentrations of CH_3 and C_2H_2 saturate above 3% CH_4, the depletion of hydrogen leads to a decrease in the growth rates at high CH_4 concentrations.

Another factor that is important in determining growth behavior on different surface orientations is the surface termination and surface atomic structure. One of the primary advantages of a three-dimensional atomic-scale growth model is that these effects are built-in, and by using a consistent set of surface chemical kinetic data like that in Table 1, the growth behavior on different surfaces of various orientations can be predicted and compared. Growth on the (100)(2×1) surface is considerably faster than on the (111) or (11 9 10) surfaces in Figure 3. This is because the addition of diamond material onto the smooth (100)(2×1) surface requires the deposition of only one carbon atom from the gas, whereas, growth on the (111) surface requires three carbon atoms.[49] However, growth at step edges on the (111) surface can occur by the addition of two or one carbon atoms (depending on the step-edge site). The (11 9 10) surface is essentially a stepped (111) surface, and, therefore, the (11 9 10) growth rate shown in Figure 3 is higher than the (111) growth rate.

This difference could be important in practice, since real substrates are rarely perfectly flat, but instead are usually miscut and contain steps. This model does not differentiate (as yet) between growth on a flat (100) surface and growth at a step on the (100) surface, so a slight miscut from the (100) orientation will not affect the (100) growth behavior. However, miscutting the (111) face by 4.7° to a (11 9 10) orientation has a significant effect on the growth rate, because growth at the steps on the miscut surface is more rapid than layer nucleation on a flat (111) face.[49] The difference between the (111) and (hkl) growth rates, where (hkl) is a surface orientation that is miscut from (111), should increase as the degree of miscut and, therefore, the density of step-edge sites on the surface increase.

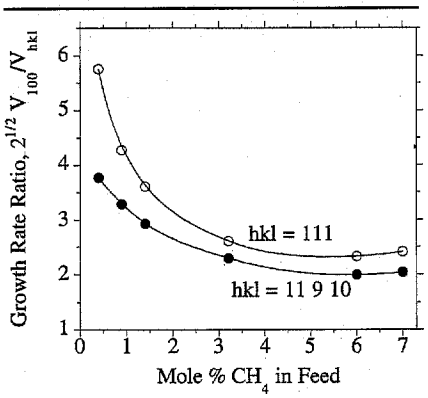

Figure 6. Growth-rate parameter for hkl = 111 and hkl = 11 9 10 [near-(111)] as a function of the concentration of methane in the feed gas.

MICROSTRUCTURAL MODELING

The relative rates of growth of the {100} and {111} faces, expressed by the growth-rate parameter α_{3D}, determine the shape that a diamond crystal will assume as it grows. This single-crystal shape will, in turn, control the microstructure of a polycrystalline film that is formed from the growth of many randomly oriented single-crystal nuclei. As depicted in Figure A in the sidebar, the idiomorphic crystal shape in two dimensions varies as α_{2D} changes between one and two. When α_{2D} is less than or equal to one, only {10} edges bound the square crystal, and only {11} edges are present when α_{2D} is greater than or equal to two.

Figure 4 shows the film microstructures for three values of α_{2D}. Under conditions similar to those found in the atomistic simulations, α_{2D} is greater than or equal to two, and the film surface is strongly peaked with mostly {11} facets (in agreement with the idiomorphic crystal shape). On the other hand, for α_{2D} slightly less than two, both {11} and {10} facets are observed. As the film grows, the crystallographic texture sharpens, and the fraction of the facets that are {10} oriented increase. At very large film thicknesses, these {10} facets orient parallel to the substrate dominate, and the film starts to become flat. The {10} facets parallel to the substrate continue to widen as the simulation progresses, and eventually the film would become very flat with predominantly {10} facets. Wild et al.[43] predict similar microstructures under the same conditions. For $\alpha_{2D} = 1.5$, both {11} and {10} facets appear in nearly equal fractions, and the film surface is flatter than for $\alpha_{2D} = 2$. For α_{2D} between 1.0 and $\sqrt{2}$, the surface morphology and microstructures are indistinguishable from those obtained between $\sqrt{2}$ and 2.0, except that the facet orientations are switched (i.e., {10} must be substituted for {11}, and vice versa).

For all values of α_{2D} examined, the grain size increases with distance from the substrate as a result of competition between adjacent facets. Near the substrate, the rate at which the grain size increases with film thickness clearly decreases as the film grows. A fit to the grain size R versus height h suggests that $R = h^{\beta}$, where $\beta = 0.5 \pm 0.15$.

The relative chance of a facet surviving depends on its orientation (relative to the substrate) and its velocity, as compared with the nearest facet in the adjacent grain. Similarly, the relative chance of a particular grain surviving depends on its orientation relative to that of its neighboring grains and the value of α_{2D}. Therefore, as the film thickness increases,

the distribution of grain orientations evolves. Figure 5 shows a series of distributions of the grain orientations (crystallographic texture) for different values of α_{2D} at a film thickness 204 times larger than the mean nuclei spacing on the substrate (204 d_o). As α_{2D} increases from one to two, the most probable grain orientation decreases from 45° (<11> out-of-plane texture) to 0° (<10> out-of-plane texture).

The idiomorphic crystal shapes in Figure A indicate that at $\alpha_{2D} = 2.0$, only {11} edges are present and the direction of fastest growth is <10>. Thus, the nuclei that are oriented with a <10> direction parallel to the growth direction grow faster than the others in that direction. Eventually, these nuclei overgrow the others, and all the grains in the film in Figure 4a are oriented with a fast-growing <10> direction pointed in the direction of growth (i.e., the film has a <10> out-of-plane texture). However, the surface of the film contains only {11} facets that are inclined to the substrate by an angle of approximately 45° (i.e., the surface morphology is jagged with {11} facets). For the same reasons, the film at $\alpha_{2D} = 1.0$ has a <11> texture with jagged surface features and {10} facets. The fastest growing direction at $\alpha_{2D} = 1.95$ is just off of <10>, and so the film in Figure 4b has a near <10> texture. However, each crystal retains small {10} edges, and these edges are nearly parallel to the substrate. Eventually these {10} edges grow together to produce the near <10> textured {10} faceted film. When $\alpha_{2D} = 1.5$, the direction of fastest growth is between <10> and <11> (near <12>), and nearly equal lengths of {10} and {11} facets are present. Thus, the film in Figure 4c is near <12> textured with a jagged surface morphology (though less so than when $\alpha_{2D} = 1.0$ or 2.0) and both {10} and {11} surface facets.

Figure 3 indicates that the (100) orientation grows significantly faster than the (111) or (11 9 10) orientations. Assigning the (100) growth rates to the {10} edge and the (111) or (11 9 10) rates to {11} yields high values of α_{2D} (Figure 7). Since growth on the (11 9 10) surface is faster than on the (111) surface, α_{2D} is lower if it is assumed that the (111) surfaces contain some supply of growth sites (due to steps, defects, etc.) like those on the (11 9 10) surface. Nonetheless, the values of α_{2D} are greater than two over most of the range of inlet CH_4 concentrations, and, thus, mostly polycrystalline films like those in Figure 4a might be expected under the conditions detailed. However, if it is assumed the {111} surfaces contain features at which growth is favored [e.g., steps as on the (11 9 10) surface], then films like that in Figure 4b for high-inlet CH_4 concentrations for which α_{2D} in Figure 6 is slightly below two might be expected.

CONCLUSIONS

It is not possible to construct a single model that can capture the physics of the diamond thin-film deposition process across a range of length scales spanning ten orders of magnitude. Instead, different types of models must be constructed, each one appropriate to a specific range of length and time scales. Molecular-growth models may be constructed based on the kinetic Monte Carlo technique. Continuum models are based on conservation equations for mass, momentum, and energy. To bridge the length-scale gap between the molecular and continuum approaches, it is necessary to implement models that describe the evolution of microstructure and morphology. The models associated with the three length-scale regimes are tightly coupled to one another through the mass and energy flux conservation conditions applicable at the deposition surface. This coupling necessitates that the three different length-scale ranges be considered simultaneously. By the same token, the solutions for the three different scales provide a clear picture of diamond deposition. Nonetheless, further work is required. More development is needed to extend the microstructural model to three dimensions, the gas-phase model to more complete spatially resolved descriptions of the reactor, and the atomic model to include twinning and additional growth mechanisms.

ACKNOWLEDGEMENTS

The authors gratefully acknowledge the support of the U.S. Advanced Research Projects Agency and the U.S. Naval Research Laboratory under contract number N00014-96-1-G000. The authors thank J.E. Schnitker for enlightening discussions.

References

1. R.C. DeVries, *Ann. Rev. Mater. Sci.*, 17 (1987), pp. 161–187.
2. F.G. Celii and J.E. Butler, *Ann. Rev. Phys. Chem.*, 42 (1991), pp. 643–684.
3. J.E. Butler and R.L. Woodin, *Phil. Trans. R. Soc. Lond. A*, 342 (1993), pp. 209–224.
4. K.E. Spear and J.P. Dismukes, eds., *Synthetic Diamond: Emerging CVD Science and Technology, Electrochemical Society Series* (New York: Wiley, 1994).
5. M.A. Prelas, G. Popovici, and L.K. Bigelow, *Handbook of Industrial Diamonds and Diamond Films* (New York: Dekker, 1997).
6. J.E. Field, *The Properties of Natural and Synthetic Diamond* (London: Academic Press, 1992).
7. J.C. Angus and C.C. Hayman, *Science*, 214 (1988), pp. 913–921.
8. M. Frenklach and K.E. Spear, *J. Mater. Res.*, 3 (1988), pp. 133–140.
9. M. Frenklach and H. Wang, *Phys. Rev. B*, 43 (1991), pp. 1520–1545.
10. D.G. Goodwin and J.E. Butler, *Handbook of Industrial Diamonds and Diamond Films*, ed. M.A. Prelas, G. Popovici, and L.K. Bigelow (New York: Dekker, 1997), pp. 527–582.
11. T. DebRoy et al., *J. Appl. Phys.*, 68, (1990), pp. 2424–2432.
12. S.J. Harris and A.M. Weiner, *J. Appl. Phys.*, 67 (1990), pp. 6520–6526.
13. M.E. Coltrin and D.S. Dandy, *J. Appl. Phys.*, 74 (1993), pp. 5803–5820.
14. D.S. Dandy and M.E. Coltrin, *J. Appl. Phys.*, 76 (1994), pp. 3102–3113.
15. D.S. Dandy and M.E. Coltrin, *Appl. Phys. Lett.*, 66 (1995), pp. 391–393.
16. H.R. Thorsheim and J.E. Butler, *Synthetic Diamond: Emerging CVD Science and Technology*, ed. K.E. Spear and J.P. Dismukes (New York: Wiley, 1994), pp. 193–242.
17. L.L. Connell et al., *J. Appl. Phys.*, 78 (1995), pp. 3622–3634.
18. D.D. Koleske et al., *J. Chem. Phys.*, 102 (1995), pp. 992–1002.
19. J.E. Butler et al., *Wide Band Gap Electronic Materials*, ed. M.A. Prelas, G. Popovici, and L.K. Bigelow (New York: Kluwer Academic, 1995), pp. 105–114.
20. B.D. Thomas and J.E. Butler, *Surf. Sci.*, 328 (1995), pp. 291–301.
21. J.A. Miller and C.T. Bowman, *Prog. Energy Combust. Sci.*, 15 (1989), p. 287.
22. J.A. Miller and C.F. Melius, *Combust. Flame*, 91 (1992), p. 21.
23. C.T. Bowman et al., *GRI-Mech*, http://www.me.berkeley.edu/gri_mech/ (1996).
24. D.G. Goodwin and G.G. Gavillet, *J. Appl. Phys.*, 68 (1990), pp. 6393–6400.
25. E. Meeks et al., *Combustion and Flame*, 92 (1993), pp. 144–160.
26. B.W. Yu and S.L. Girshick, *J. Appl. Phys.*, 75 (1994), pp. 3914–3923.
27. N.G. Glumac and D.G. Goodwin, *Combustion and Flame*, 105 (1996), p. 321.
28. K. Tankala and T.K. DebRoy, *J. Appl. Phys.*, 72 (1992), pp. 712–718.
29. Y.A. Mankelevich, A.T. Rakhimov, and N.V. Suetin, *Diam. Rel. Mater.* 4 (1995), pp. 1065–1068.
30. Y.A. Mankelevich, A.T. Rakhimov, and N.V. Suetin, *Diam. Rel. Mater.* 5 (1996), pp. 888–894.
31. K. Hassouni et al., *J. de Physique III*, 6 (1996), pp. 1229–1243.
32. E. Hyman et al., *J. of Vac. Sci. and Tech.*, A, 12 (1994), pp. 1474–1799.
33. D.N. Belton and S.J. Harris, *J. Chem. Phys.*, 96 (1992), pp. 2371–2377.
34. S.J. Harris and D.G. Goodwin, *J. Phys. Chem.*, 97 (1993), pp. 23–28.
35. D.S. Dandy and M.E. Coltrin, *J. Mater. Res.*, 10 (1995), pp. 1993–2010.
36. E.J. Dawnkaski, D. Srivastava, and B.J. Garrison, *J. Chem. Phys.*, 104 (1996), pp. 5997–6008.
37. M.M. Clark, L.M. Raff, and H.L. Scott, *Comp. in Phys.*, 10 (1996), pp. 584–590.
38. B.J. Garrison et al., *Science*, 255 (1992), pp. 835–838.
39. S. Skokov, B. Weiner, and M. Frenklach, *J. Phys. Chem.*, 99 (1995), pp. 5616–5625.
40. C.C. Battaile, D.J. Srolovitz, and J.E. Butler, *J. Appl. Phys.*, in press.
41. A.B. Bortz, M.H. Kalos, and J.L. Lebowitz, *J. Comp. Phys.*, 17 (1975), pp. 10–18.
42. K.E. Spear, *J. Amer. Ceram. Soc.*, 72 (1989), pp. 171–191.
43. C. Wild et al., *Diam. Rel. Mater.*, 2 (1993), pp. 158–168.
44. G.V. Saparin, *Diam. Rel. Mater.*, 3 (1994), pp. 1337–1351.
45. W.L. Hsu, *Appl. Phys. Lett.*, 59, (1991), pp. 1427–1429.
46. C. Wolden, S. Mitra, and K.K. Gleason, *J. Appl. Phys.*, 72 (1992), pp. 3750–3758.
47. D.G. Goodwin, *Appl. Phys. Lett.*, 59 (1991), pp. 277–279.
48. Y.A. Mankelevich, A.T. Rakhimov, and N.V. Suetin, *Plasma Phys. Rep.*, 21 (1995), p. 872.
49. C.C. Battaile, D.J. Srolovitz, and J.E. Butler, *Diam. Rel. Mater.*, in press.

ABOUT THE AUTHORS

David J. Srolovitz earned his Ph.D. in materials science and engineering at the University of Pennsylvania in 1981. He is currently Edward DeMille Campbell Professor of Materials Science and Engineering and professor of applied sciences at the University of Michigan. Dr. Srolovitz is also a member of TMS.

David S. Dandy earned his Ph.D. in chemical engineering at California Institute of Technology in 1987. He is currently a professor of chemical and bioresource engineering at Colorado State University.

James E. Butler earned his Ph.D. in chemical physics at the University of Chicago in 1972. He is currently head of the Gas/Surface Dynamics Section at the Naval Research Laboratory.

Corbett C. Battaile earned his M.S. in materials science and engineering at Vanderbilt University in 1992. He is currently a graduate student and research assistant at the University of Michigan. Mr. Battaile is also a member of TMS.

Paritosh earned his B.E. in chemical engineering at the University of Roorkee, India, in 1993. He is currently a graduate student and research assistant at the University of Michigan.

For more information, contact D.J. Srolovitz, University of Michigan, 3062 Dow Building, Ann Arbor, Michigan 48109-2136; (313) 936-1470; fax (313) 763-4788; e-mail srol@umich.edu.